Effect of laser wavelength on phase and microstructure of TiO_2 films prepared by laser chemical vapor deposition

Ming Gao, Akihiko Ito*, Takashi Goto

Institute for Materials Research, Tohoku University, 2-1-1 Katahira, Aoba-ku, Sendai 980-8577

**corresponding author: e-mail: itonium@imr.tohoku.ac.jp*

tel: +81-22-215-2106; fax: +81-22-215-2107

Abstract: Rutile and anatase TiO_2 films were prepared by laser chemical vapor deposition using CO_2 and Nd:YAG lasers. The effects of laser wavelength on the phase, orientation, and microstructure of these TiO_2 films were investigated. Using a CO_2 laser, single-phase rutile TiO_2 films were obtained at 826–1225 K. These films showed a (100) orientation and a dense structure. The highest deposition rate was 83 μm h^{-1} at 1070 K. Using a Nd:YAG laser, the phase of the TiO_2 films changed from rutile to anatase with increasing deposition temperature from 852 to 1230 K. The rutile TiO_2 films showed a (100) orientation with a columnar structure, while the anatase TiO_2 films exhibited a (001) orientation with a cauliflower-like structure. Using a Nd:YAG laser, the highest deposition rates for rutile and anatase TiO_2 films were 142 and 40 μm h^{-1}, respectively.

Keywords: Laser CVD, Anatase, Rutile, Thick film

Please cite this manuscript as

M. Gao, A. Ito, T. Goto: Effect of laser wavelength on phase and microstructure of TiO_2 films prepared by laser chemical vapor deposition, *Surface and Coatings Technology* **244(15)** 166–172 (2014). doi:10.1016/j.surfcoat.2014.02.003

This is the accepted version of the article submitted to Surface and Coatings Technology, which has been published in final form at 10.1016/j.surfcoat.2014.02.003.

1. Introduction

TiO_2 films have been extensively studied because of their photocatalytic, photovoltanic, and optical properties [1, 2], and thus have been widely applied to hydrogen generation [3], purification of polluted water [4], and self-cleaning of optical device windows and waveguides. TiO_2 has several polymorphs, mainly anatase and rutile, which could be low- and high-temperature phases, respectively [5]. The photocatalytic and photovoltanic performance of anatase or an anatase/rutile mixture of TiO_2 is superior to that of rutile TiO_2 [6, 7], while highly crystalline rutile TiO_2 can be used for optical applications.

TiO_2 films can be prepared by several physical and chemical deposition processes. Metalorganic chemical vapor deposition (MOCVD) has been widely used to prepare TiO_2 films because of its good conformal coverage and applicability to large-scale industrial production. Anatase TiO_2 films are usually obtained at deposition temperatures less than about 800 K, which results in low crystallinity and deposition rates less than a few μm h^{-1} [7–13]. The photocatalytic and optical properties of TiO_2 films depend on crystallinity and crystal orientation [14]. Therefore, highly crystalline rutile and anatase TiO_2 films should be prepared at high deposition rates.

Auxiliary-energy-assisted CVD processes such as plasma CVD and photo CVD are useful for obtaining highly crystalline films. Laser-assisted CVD (laser CVD) has been employed to prepare various oxide and carbide films [15–17], including thick TiO_2 films [18,19]. Laser CVD can be categorized into two types: photolytic laser CVD and pyrolytic laser CVD. Photolytic laser CVD can prepare amorphous films without heating the substrate [20,21], while pyrolytic laser CVD can prepare highly crystalline films [22,23]. CO_2 lasers are often used for pyrolytic laser CVD; however, no research has been reported on the preparation of TiO_2 films by this method. Nd:YAG is an near-infrared laser and has photon energy higher than that of a CO_2 laser. Laser CVD using a Nd:YAG laser may be a fundamentally pyrolytic laser CVD process. However, the differences in the deposition features using CO_2 and Nd:YAG lasers have never been studied.

In the present study, TiO_2 films were prepared by laser CVD using CO_2 and Nd:YAG lasers, and the effects of deposition conditions and laser wavelength on the orientation and microstructure of TiO_2 films were investigated.

2. Experimental procedures

Figure 1 depicts a schematic of the laser CVD apparatus. Titanium di(*i*-propoxy)–bis(dipivaloylmethanate) ($Ti(OiPr)_2(dpm)_2$) as a precursor was heated at 453 K, and its vapor was carried into the CVD chamber through an Ar carrier gas. O_2 gas was separately introduced into the CVD chamber through a double-tube nozzle. The gas flow rates of the Ar and O_2 gases were each maintained at 1.6×10^{-7} m^3 s^{-1}. The total pressure (P_{tot}) was varied from 0.2 to 0.8 kPa. Yttria-stabilized zirconia (YSZ) plates (5 mm × 5 mm × 1 mm) were used as substrates, which were preheated on a hot stage to 673 K. A Nd:YAG laser (wavelength: 1.06 μm) and a CO_2 laser (wavelength: 10.6 μm) in continuous wave modes were,

This is the accepted version of the article submitted to Surface and Coatings Technology, which has been published in final form at 10.1016/j.surfcoat.2014.02.003.

respectively, used to irradiate the entire substrate through a quartz and ZnSe window. The deposition temperature (T_{dep}) was measured with a thermocouple inserted into the back side of the substrate. The deposition time was fixed at 0.6 ks.

The phase was determined by X-ray diffraction (XRD; Rigaku RAD-2C, 30 kV and 20 mA). The surface and cross-sectional microstructures were observed by a scanning electron microscope (SEM; Hitachi S-3100H). The thickness was measured from a cross-sectional SEM image. The deposition rate (R_{dep}) was calculated from the thickness and deposition time. The crystal structure was schematically illustrated using the VESTA software package [24]. The Harris texture coefficient (*TC*) was used to estimate the orientation of the obtained films [25,26].

$$TC(hkl) = N\frac{I_m(hkl)/I_0(hkl)}{\sum I_m(hkl)/I_0(hkl)}, \qquad (1)$$

where I_m(hkl) and I_0(hkl) are the intensity from the (*hkl*) plane measured in the present study and that reported on the ICSD card, respectively. For the rutile TiO_2 phase (ICSD #9161; space group: $P4_2/mnm$; a = 0.4564 nm, c = 0.2959 nm), the (110), (101), (200), (111), (211), (002), (310), (301), and (210) planes were used for the calculation (N = 9). For the anatase TiO_2 phase (ICSD #9852; space group: $I4_1/amd$; a = 0.3784 nm, c = 0.9515 nm), the (101), (103), (004), (112), (200), (105), (204), (211), and (220) planes were used for the calculation (N = 9). The texture coefficient *TC*(*hkl*) has a value between 0 and *N* depending on the orientation degree of the (*hkl*) plane. The *TC*s of perfectly oriented and non-oriented planes are *N* and 1.0, respectively. In the present study, if the *TC*(*hkl*) value is more than 2, the film is defined as (*hkl*) oriented. $TC(hkl)_R$ and $TC(hkl)_A$ refer to the texture coefficients of rutile and anatase TiO_2 films, respectively.

3. Results and discussion

3.1 Preparation of TiO_2 films using a CO_2 laser

The XRD patterns of all films prepared using a CO_2 laser can be indexed as single-phase rutile TiO_2. Figure 2 shows the XRD patterns of TiO_2 films prepared at a pressure of 0.4 kPa. The rutile TiO_2 films prepared at T_{dep} = 1020 K had a (100) orientation (Fig. 2(a)). $TC(100)_R$ slightly decreased from 3.6 to 1.4 with increasing T_{dep} from 870 to 1217 K (Fig. 2(b)). $TC(110)_R$ was around 1, and thus no orientation toward the (110) plane was identified. The (100) orientation observed for rutile TiO_2 films was independent of P_{tot}. Figure 3 depicts the effect of T_{dep} on $TC(hkl)_R$ for rutile TiO_2 films prepared at P_{tot} = 0.4 kPa. $TC(100)_R$ was highest among other $TC(hkl)_R$ values independent of T_{dep} and P_{tot}, and $TC(100)_R$ slightly decreased with increasing T_{dep}. $TC(310)_R$ and $TC(210)_R$ were almost 2, while $TC(110)_R$ and $TC(101)_R$ were almost 1 and 0, respectively. Therefore, the (100) orientation was dominant independent of the deposition conditions.

Figure 4 shows the surface and cross-sectional SEM images of the TiO_2 films. The rutile TiO_2 film prepared at P_{tot} = 0.8 kPa and T_{dep} = 853 K had a pebble-like structure and columnar cross section (Fig. 4(a), 4(b)). The rutile TiO_2 film prepared at P_{tot} = 0.2 kPa and T_{dep} = 1078 K consisted of faceted polygonal grains and a dense cross section (Fig. 4(c), 4(d)).

This is the accepted version of the article submitted to Surface and Coatings Technology, which has been published in final form at 10.1016/j.surfcoat.2014.02.003.

The rutile TiO_2 faceted grains in the present study were categorized into three types: A, B, and C, as shown in Fig. 4(c). Grain type A had a truncated two-sided surface that could be indexed as a {110} facet with {001} facets truncated by {201} planes (Fig. 5(a)). Grain type B showed a quadrangular pyramidal shape where two sides had a double slope. These grains could be indexed as {110} and {001} facets truncated by {201} and {101} planes (Fig. 5(b)). Grain type C had a two-sided double slope surface. The surface facets could be indexed as (301) and (101) planes, and the vertical facet could be indexed as {110} plane (Fig. 5(c)). The first principles calculated surface energies of the (110), (100), (001), and (011) planes [27], and the (110) surface had the lowest energy. Therefore, the (110) plane likely appeared as a roof facet on the (100)-oriented rutile TiO_2 grains, and the (*h*01) planes (h = 1–3) could be truncated by the (110) planes, as depicted in Fig. 5.

Figure 6 summarizes the effect of the deposition conditions (T_{dep} and P_{tot}) on the phase and microstructure of TiO_2 films prepared using a CO_2 laser. Single-phase rutile TiO_2 films were obtained independent of T_{dep} and P_{tot}. The microstructure changed from dense columnar to fully dense with increasing T_{dep}.

Figure 7 shows the relationship between T_{dep} and R_{dep} in an Arrhenius plot form. At P_{tot} = 0.2 kPa, R_{dep} increased from 13 to 83 μm h^{-1} with T_{dep} increasing from 878 to 1070 K, and decreased to 32 μm h^{-1} at 1233 K, showing the maximum value at 1070 K. At lower deposition temperatures, the deposition rate increased with increasing deposition temperature, suggesting a reaction limited process. The activation energy of the deposition was 46–63 kJ mol^{-1}. These values are similar to those given in the literature for TiO_2 films prepared by conventional MOCVD (41–88 kJ mol^{-1}) [11,13,28,29]. With increasing P_{tot}, the maximum R_{dep} slightly decreased, and the T_{dep} providing for the maximum R_{dep} also decreased. This trend has been commonly observed in conventional CVD, *i.e.*, a homogeneous gas phase reaction results in a decrease in the deposition rate at high temperatures.

3.2 Preparation of TiO_2 films using Nd:YAG laser

Figures 8 shows XRD patterns of TiO_2 films prepared at P_{tot} = 0.6 kPa using a Nd:YAG laser. A single-phase rutile TiO_2 film having (100) orientation was obtained at T_{dep} = 1020 K ($TC(200)_R$ = 4.0) (Fig. 8(a)). A mixture of rutile and anatase TiO_2 films was formed at T_{dep} = 1072 K (Fig. 8(b)). Single-phase anatase TiO_2 films were prepared above T_{dep} = 1142 K and exhibited a (001) orientation ($TC(004)_A$ = 4.5) (Fig. 8(c)).

Figure 9 depicts the effect of T_{dep} on $TC(hkl)_R$ and $TC(hkl)_A$ for TiO_2 films prepared at P_{tot} = 0.6 kPa. With increasing T_{dep}, the phase of the TiO_2 films changed from rutile (936–1035 K) to a mixture (1072 K) to anatase (1114–1167 K) and back to a mixture (1185 K). $TC(100)_R$ showed a maximum value of 4.0 at T_{dep} = 1035 K, and slightly decreased to 2 with increasing T_{dep} to 1185 K. $TC(101)_R$ was less than 1.2 independent of T_{dep}. On the other hand, $TC(001)_A$ ranged between 4.1 and 7.0, and $TC(101)_A$ was less than 0.5, implying that anatase TiO_2 films exhibited a significant (001) orientation.

Figure 10 shows the surface and cross-sectional SEM images of TiO_2 films prepared at P_{tot} = 0.6 kPa. The (100)-oriented rutile TiO_2 films consisted of faceted grains having a columnar cross section (Fig. 10(a), 10(b)). The (001)-oriented anatase TiO_2 films had cauliflower-like grains with a columnar cross section (Fig. 10(c), 10(d)).

Figure 11 shows the surface and cross section of the columnar grains of the (100)-oriented rutile TiO_2 film prepared at P_{tot} = 0.4 kPa and T_{dep} = 1047 K. Pyramidal facets with a step structure were developed in the columnar grains (Fig. 11(b)). The (100)-oriented columnar grain had a pyramidal cap with fourfold facets. The four sides of the pyramidal cap could be indexed as the {111} planes. A schematic of the facets and the atomic arrangement of (100)-oriented rutile TiO_2 grains (grain E in Fig. 11(a)) is illustrated in Fig. 11(c). The step structure on the facets (Fig. 11(b)) was associated with the atomic arrangement of TiO_6 octahedra on the rutile {111} plane.

In the cross section of the (100)-oriented grains (Fig. 11(d)), a triangular terrace developed on the front ridge of the columnar grains, while a shoulder facet developed on the side ridges. The triangular terrace could be indexed as $(\bar{1}20)$ planes truncated by the {111} plane. A schematic of the facets for rutile TiO_2 crystals truncated by {111}, {102}, and {120} planes was overlaid on the cross-sectional SEM images of grains F and G (Fig. 11(e), 11(f)).

Figure 12 summarizes the effect of the deposition conditions (T_{dep} and P_{tot}) on the phase and microstructure of TiO_2 films prepared using a Nd:YAG laser. Single-phase rutile TiO_2 films were obtained in the region of low T_{dep} and P_{tot} (filled circles in Fig. 12). At high T_{dep} and P_{tot}, single-phase anatase TiO_2 films were obtained and exhibited a cauliflower-like structure (open circles in Fig. 12).

Figure 13 shows the relationship between T_{dep} and R_{dep} in an Arrhenius plot form for a Nd:YAG laser. At P_{tot} = 0.4 kPa, R_{dep} increased with increasing T_{dep} up to T_{dep} = 1010 K. The values for E_a below the T_{dep} showing the maximum R_{dep} were 83–86 kJ mol^{-1} for P_{tot} = 0.2–0.8 kPa. These are similar to the values given in the literature for TiO_2 films prepared by conventional MOCVD (41–88 kJ mol^{-1}) [11,13,28,29]. The maximum R_{dep} was 142 μm h^{-1} at 1010 K.

3.3 Anatase-and-rutile formation of TiO_2 films

Figure 14 summarizes the anatase-and-rutile formation temperatures in TiO_2 films prepared by MOCVD [7–13,28–30] and the present laser CVD method. Using a titanium tetraisopropoxide (TTIP) precursor [7,8,10,11,28,29], anatase TiO_2 was obtained at T_{dep} = 450–980 K, while rutile TiO_2 formed at T_{dep} = 700–850 K. Amorphous films were obtained at a lower deposition temperature range. By using an ethylacetoacetate (ETOB) precursor [12], anatase TiO_2 films were prepared above 750 K, while amorphous TiO_2 films were obtained below 750 K. By using a dipivaloylmethanate (DPM) precursor, anatase TiO_2 films having a (001) orientation were obtained at 700–900 K [30]. We earlier prepared TiO_2 films by MOCVD, and reported that the phase changed from anatase to rutile to a mixture of rutile and anatase with increasing deposition temperature from 600 to 1100 K [13]. This anatase formation at high temperatures was also accompanied by the formation of a cauliflower-like structure. In the present study, single-phase anatase TiO_2 films were obtained at 1100–1200 K, which is the highest deposition temperature among TiO_2 films prepared by MOCVD.

Rutile TiO_2 tends to be the thermodynamically stable phase at high temperatures, and phase transition from anatase to rutile TiO_2 has been reported at 873–973 K [4] (hatched area in Fig. 14). On the other hand, for CVD, anatase TiO_2 has been often obtained at higher temperatures (773–1073 K), where the deposition rate of anatase TiO_2 films decreases with increasing deposition temperature because of powder formation in the gas phase [11,28], and anatase TiO_2 films exhibit a cauliflower-like microstructure consisting of nanosized spherical grains [13]. It has been reported that anatase TiO_2 can be stable in nanoparticles of a size less than 35 nm, which demonstrates the size effect [4]. The anatase TiO_2 film might be formed in the gas phase (at a lower temperature than that of the substrate surface) as nanoparticles, and deposited on a substrate resulting in the cauliflower-like structure.

For the present laser CVD, CO_2 laser produced only rutile TiO_2 films; however, Nd:YAG laser can produce anatase TiO_2 films even at high temperatures. CO_2 laser beam had a pyrolytic effect dominantly, and rutile TiO_2 films were obtained at whole T_{dep} region (826–1225 K). These rutile TiO_2 films exhibited a faceted dense structure as shown in Figs. 4 and 5. Adatoms on film surface had high mobility and diffused farther, and nucleation site would be steps and kinks, resulting in a significant lateral growth.

Contrary, by using Nd:YAG laser, rutile TiO_2 films grew with a feather-like columnar structure and anatase TiO_2 films formed with the cauliflower-like structure at high P_{tot} (0.6–0.8 kPa) and T_{dep} (1100–1200 K) region as shown in Fig. 10. These might be due to that homogeneous nucleation occurred on terraces or in the gas phase, resulting in a rapid vertical growth. A nucleation of anatase nanoparticle in a gas phase might be promoted due to a photolytic interaction between a precursor gas and Nd:YAG laser beam.

4. Conclusions

TiO_2 films were prepared on YSZ substrates by laser CVD. Using a CO_2 laser, single-phase rutile TiO_2 films were obtained independent of P_{tot} and T_{dep}. The microstructure of single-phase (100)-oriented rutile TiO_2 films changed from columnar to dense with increasing T_{dep} and exhibited faceted morphologies. Using a Nd:YAG laser, the phase of TiO_2 films changed from a (100)-oriented rutile to a (001)-oriented anatase with increasing T_{dep} and P_{tot}, and their microstructure changed from columnar to feather-like to cauliflower-like structure. The highest R_{dep} values for rutile and anatase TiO_2 films were 142 and 40 μm h^{-1}, respectively. Anatase TiO_2 films grew with a cauliflower-like structure even at high temperatures, where anatase TiO_2 was nucleated in a gas phase and stabilized as nanoparticles.

Acknowledgements

This research was supported in part by the Global COE Program of Materials Integration, Tohoku University, and in part by the Japan Society for the Promotion of Science, Grant-in-Aid for Young Scientists

(A), 25709069. This research was also supported in part by in part by the 111 project, China (B13035).

References

[1] A. Fujishima, T.N. Rao, D.A. Tryk, Titanium dioxide photocatalysis, J. Photochem. Photobiol. C. 1 (2000) 1–21.

[2] J. Nowotny, T. Bak, M.K. Nowotny, L.R. Sheppard, Titanium dioxide for solar-hydrogen I. Functional properties, Int. J. Hydrogen Energ. 32 (2007) 2609–2629.

[3] M. Ni, M.K.H. Leung, D.Y.C. Leung, K. Sumathy, A review and recent developments in photocatalytic water-splitting using for hydrogen production, Renew. Sustain. Energ. Rev. 11 (2007) 401–425.

[4] D. Hanaor, C. Sorrell, Review of the anatase to rutile phase transformation, J. Mater. Sci. 46 (2011) 855–874.

[5] J. Augustynski, The role of the surface intermediates in the photoelectrochemical behaviour of anatase and rutile TiO_2, Electrochimica Acta. 38 (1993) 43–46.

[6] A. Sclafani, J.M. Herrmann, Comparison of the Photoelectronic and Photocatalytic Activities of Various Anatase and Rutile Forms of Titania in Pure Liquid Organic Phases and in Aqueous Solutions, J. Phys. Chem. 100 (1996) 13655–13661.

[7] T. Fuyuki, H. Matsunami, Electronic Properties of the Interface between Si and TiO_2 Deposited at Very Low Temperatures, Jpn. J. Appl. Phys. 25 (1986) 1288–1291.

[8] D. Byun, Y. Jin, B. Kim, J. Kee Lee, D. Park, Photocatalytic TiO_2 deposition by chemical vapor deposition, J. Hazard. Mater. 73 (2000) 199–206.

[9] J.-P. Lu, J. Wang, R. Raj, Solution precursor chemical vapor deposition of titanium oxide thin films, Thin Solid Films. 204 (1991) L13–L17.

[10] C. Byun, J.W. Jang, I.T. Kim, K.S. Hong, B.-W. Lee, Anatase-to-rutile transition of titania thin films prepared by MOCVD, Mater. Res. Bull. 32 (1997) 431–440.

[11] S. Krumdieck, R. Raj, Growth rate and morphology for ceramic films by pulsed-MOCVD, Surf. Coat. Technol. 141 (2001) 7–14.

[12] K. Shalini, S. Chandrasekaran, S.A. Shivashankar, Growth of nanocrystalline TiO_2 films by MOCVD using a novel precursor, J. Cryst. Growth. 284 (2005) 388–395.

[13] R. Tu, T. Goto, High Temperature Stability of Anatase Films Prepared by MOCVD, Mater. Trans. 49 (2008) 2040–2046.

[14] A. Fujishima, X. Zhang, D.A. Tryk, TiO_2 photocatalysis and related surface phenomena, Surface Science Reports. 63 (2008) 515–582.

[15] T. Goto, R. Banal, T. Kimura, Morphology and preferred orientation of Y_2O_3 film prepared by high-speed laser CVD, Surf. Coat. Technol. 201 (2007) 5776–5781.

[16] H. Kadokura, A. Ito, T. Kimura, T. Goto, Moderate temperature and high-speed synthesis of α-

Al_2O_3 films by laser chemical vapor deposition using Nd:YAG laser, Surf. Coat. Technol. 204 (2010) 2302–2306.

[17] K. Fujie, A. Ito, R. Tu, T. Goto, Laser chemical vapor deposition of SiC films with CO_2 laser, J. Alloys Compd. 502 (2010) 238–242.

[18] M. Gao, A. Ito, R. Tu, T. Goto, Microcolumnar and granular structures of TiO_2 films prepared by laser CVD using Nd:YAG laser, Key Eng. Mater. 508 (2012) 287–290.

[19] M. Gao, A. Ito, R. Tu, T. Goto, Preparation of titania solid films by laser CVD using CO_2 laser, Key Eng. Mater. 508 (2012) 279–282.

[20] T.R. Dietrich, S. Chiussi, H. Stafast, F.J. Comes, ArF laser CVD of hydrogenated amorphous silicon: The role of buffer gases, Appl. Phys. A. 48 (1989) 405–414.

[21] M. Lindstam, M. Boman, K. Piglmayer, On the growth mechanism of UV laser deposited a-C:H from CH_2I_2 at room temperature, Applied Surface Science. 172 (2001) 200–206.

[22] P.A. Molian, A. Waschek, CO_2 laser deposition of diamond thin films on electronic materials, J Mater Sci. 28 (1993) 1733–1737.

[23] C. Duty, R. Johnson, S. Bondi, W. j. Lackey, Pyrolytic Laser CVD of Boron Nitride and Molybdenum, Chemical Vapor Deposition. 9 (2003) 298–301.

[24] K. Momma, F. Izumi, VESTA 3 for three-dimensional visualization of crystal, volumetric and morphology data, J. Appl. Crystallogr. 44 (2011) 1272–1276.

[25] C.S. Barrett, T.B. Massalski, Structure of Metals, 3rd ed., McGraw-Hill Book Company, Inc., New York, 1980.

[26] A. Ito, H. Kadokura, T. Kimura, T. Goto, Texture and orientation characteristics of α-Al_2O_3 films prepared by laser chemical vapor deposition using Nd:YAG laser, J. Alloys Compd. 489 (2010) 469–474.

[27] M. Ramamoorthy, D. Vanderbilt, R.D. King-Smith, First-principles calculations of the energetics of stoichiometric TiO_2 surfaces, Phys. Rev. B. 49 (1994) 16721–16727.

[28] B.-C. Kang, S.-B. Lee, J.-H. Boo, Growth of TiO_2 thin films on Si(100) substrates using single molecular precursors by metal organic chemical vapor deposition, Surf. Coat. Technol. 131 (2000) 88–92.

[29] S. Mathur, P. Kuhn, CVD of titanium oxide coatings: Comparative evaluation of thermal and plasma assisted processes, Surf. Coat. Technol. 201 (2006) 807–814.

[30] V.G. Bessergenev, I.V. Khmelinskii, R.J.F. Pereira, V.V. Krisuk, A.E. Turgambaeva, I.K. Igumenov, Preparation of TiO_2 films by CVD method and its electrical, structural and optical properties, Vacuum. 64 (2002) 275–279.

This is the accepted version of the article submitted to Surface and Coatings Technology, which has been published in final form at 10.1016/j.surfcoat.2014.02.003.

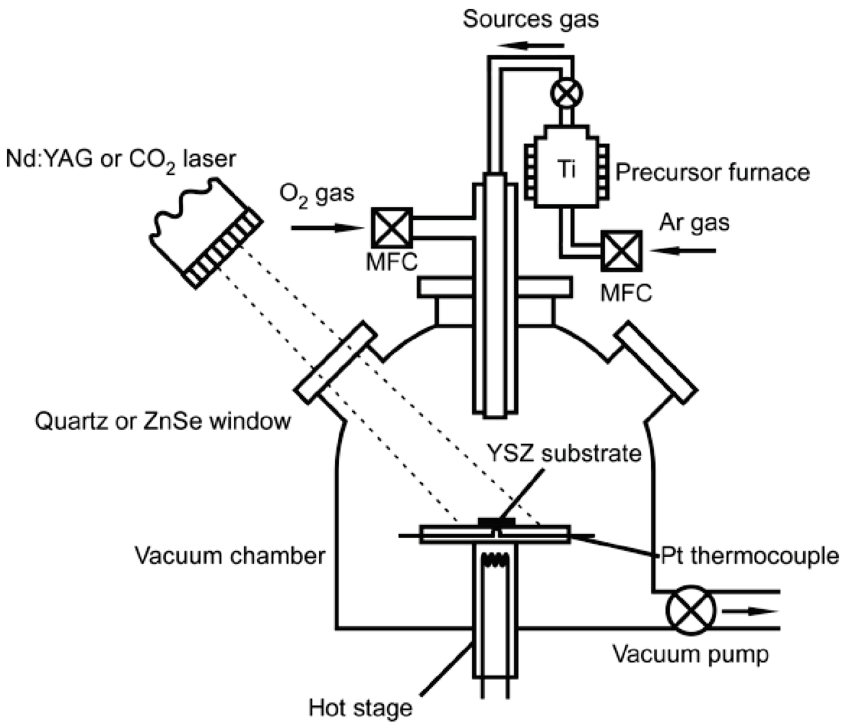

Figure 1 A schematic of laser CVD equipment.

This is the accepted version of the article submitted to Surface and Coatings Technology, which has been published in final form at 10.1016/j.surfcoat.2014.02.003.

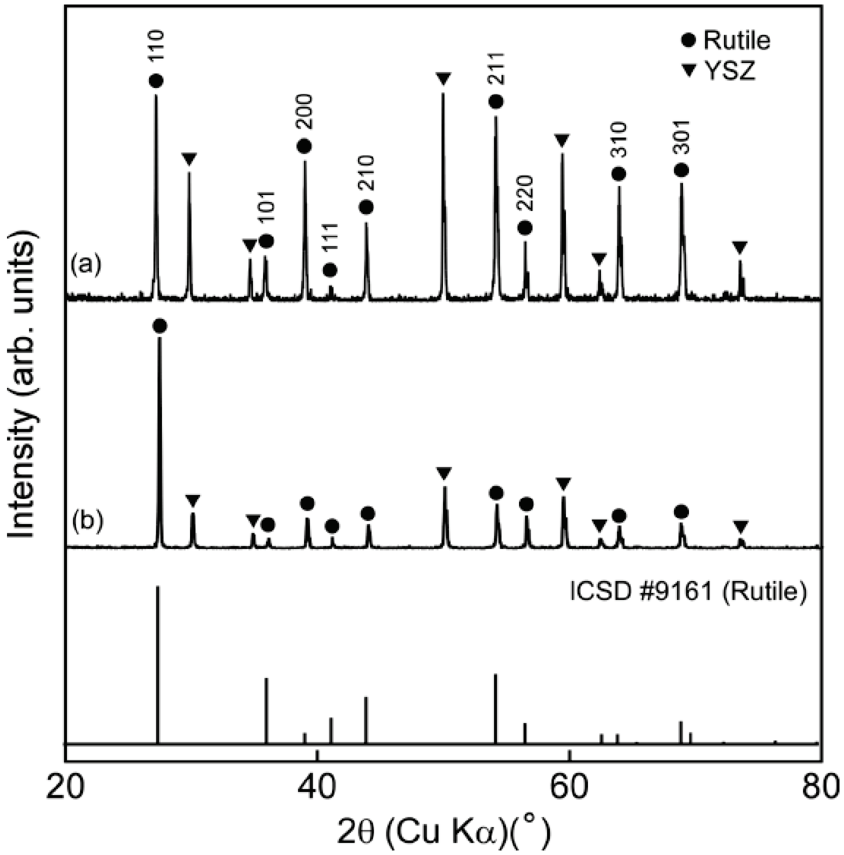

Figure 2 XRD patterns of TiO_2 films prepared using CO_2 laser at P_{tot} = 0.4 kPa and various T_{dep}: 1020 K (a) and 1078 K (b).

This is the accepted version of the article submitted to Surface and Coatings Technology, which has been published in final form at 10.1016/j.surfcoat.2014.02.003.

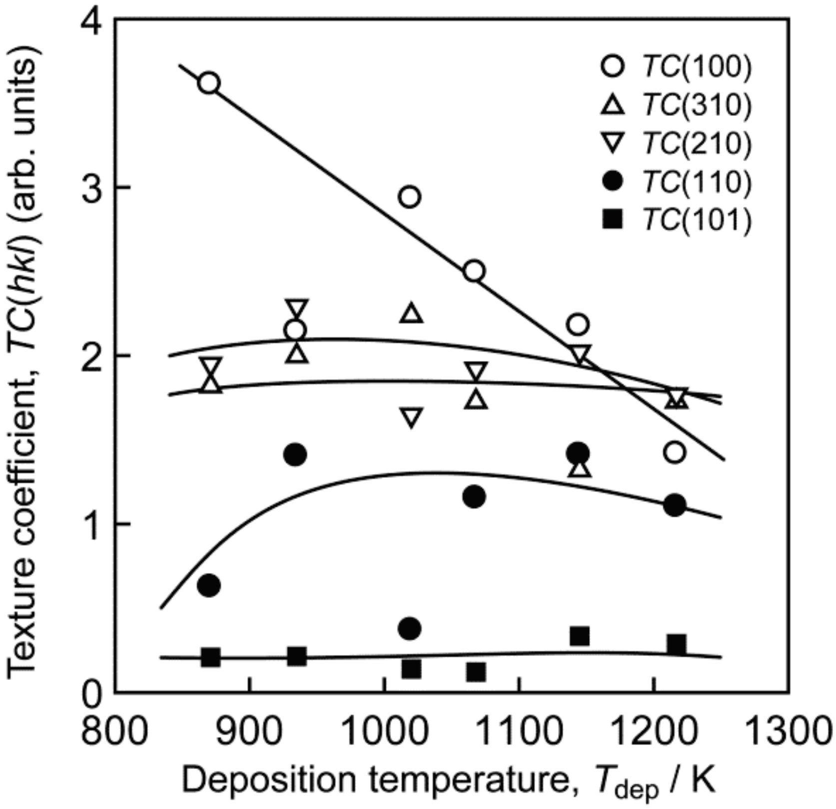

Figure 3 Effect of T_{dep} on $TC(hkl)$ of TiO_2 films prepared using Nd:YAG laser at P_{tot} = 0.6 kPa.

This is the accepted version of the article submitted to Surface and Coatings Technology, which has been published in final form at 10.1016/j.surfcoat.2014.02.003.

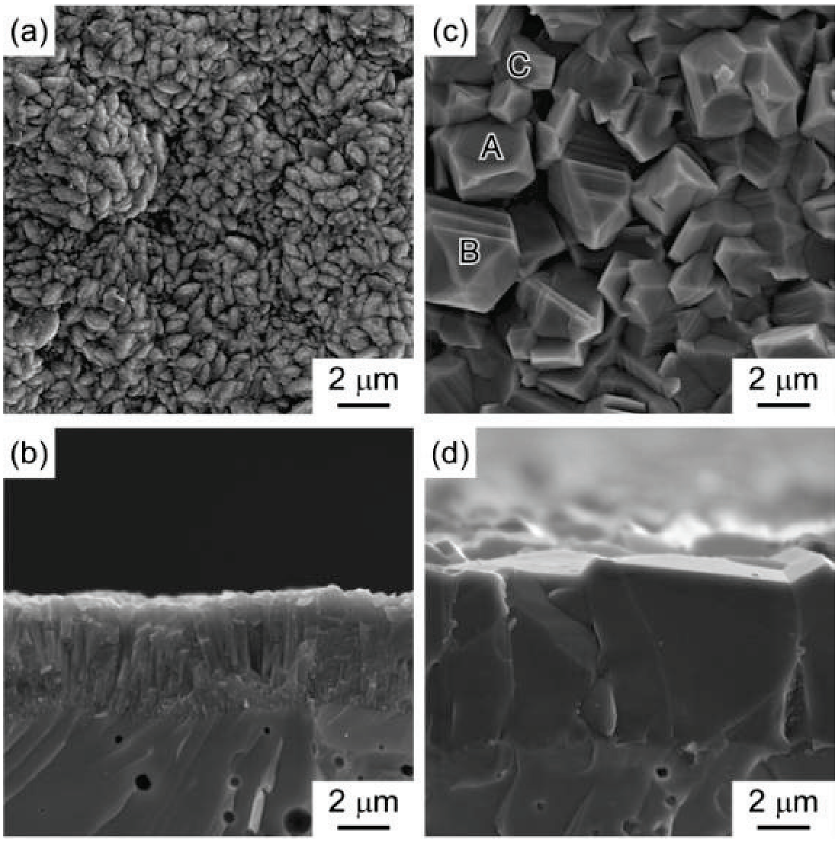

Figure 4 Surface (a, c) and cross-sectional (b, d) SEM images of TiO_2 films prepared using CO_2 laser at various P_{tot} and T_{dep}: 0.8 kPa and 853 K (a, b), 0.2 kPa and 1078 K (c, d).

This is the accepted version of the article submitted to Surface and Coatings Technology, which has been published in final form at 10.1016/j.surfcoat.2014.02.003.

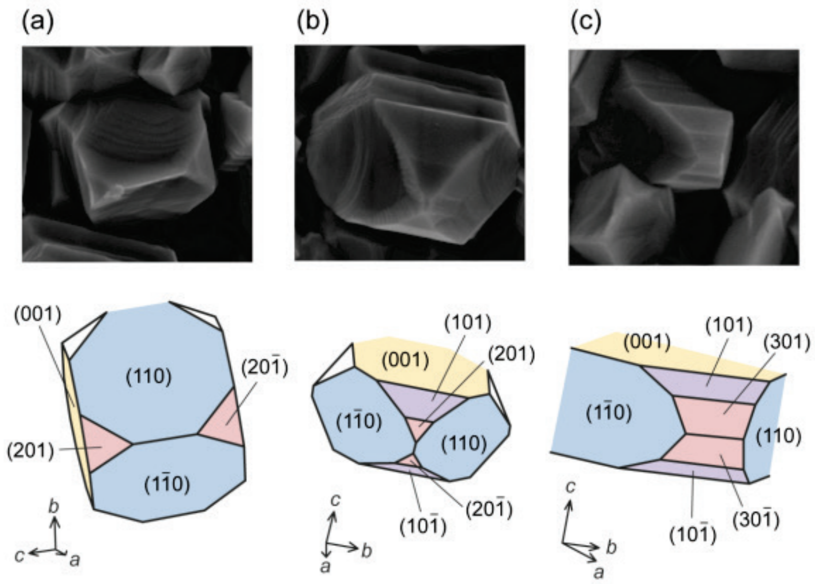

Figure 5 Pyramidal-shaped grains in the rutile TiO_2 films prepared at P_{tot} = 0.2 kPa and T_{dep} = 1078 K and their crystal shapes.

This is the accepted version of the article submitted to Surface and Coatings Technology, which has been published in final form at 10.1016/j.surfcoat.2014.02.003.

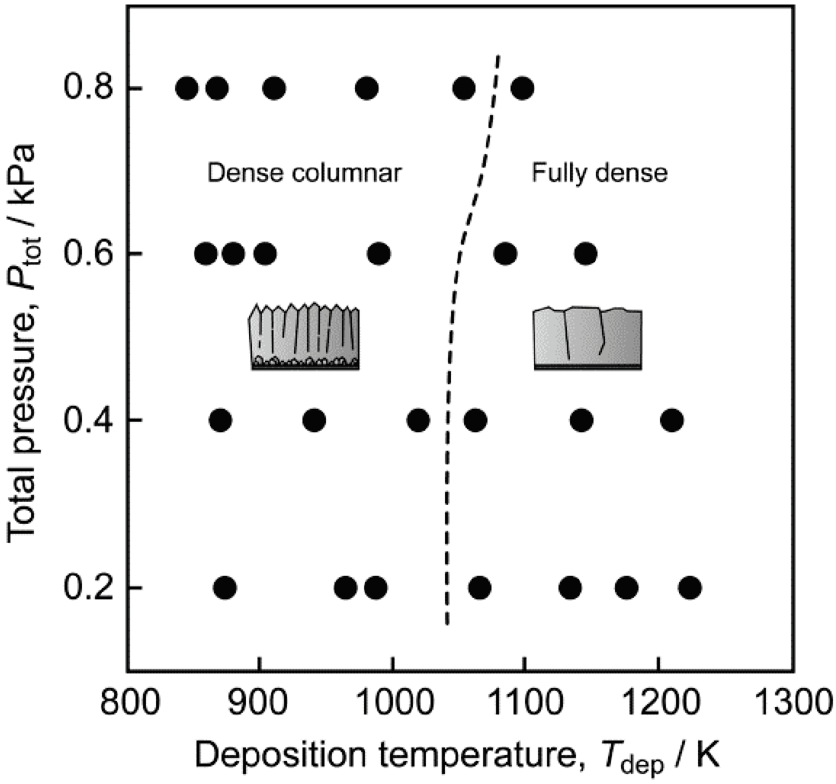

Figure 6 Effect of T_{dep} and P_{tot} on the phase and microstructure of TiO_2 films prepared using CO_2 laser. Filled circles indicate the rutile formation.

This is the accepted version of the article submitted to Surface and Coatings Technology, which has been published in final form at 10.1016/j.surfcoat.2014.02.003.

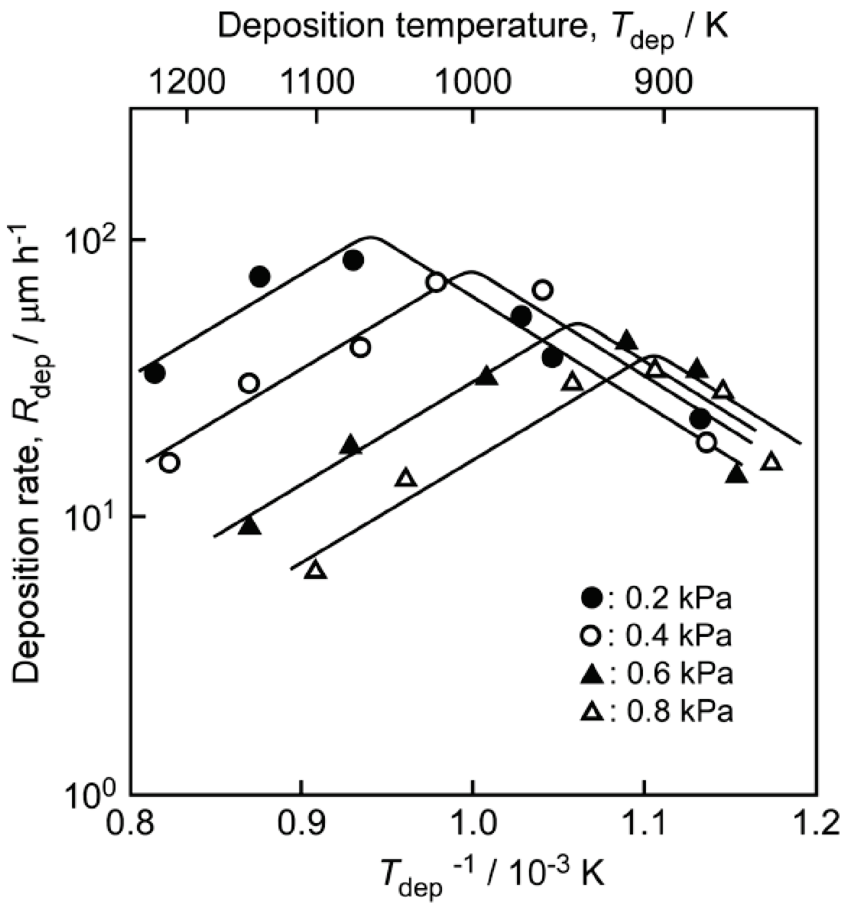

Figure 7 Effect of T_{dep} and P_{tot} on R_{dep} of TiO_2 films prepared using CO_2 laser.

This is the accepted version of the article submitted to Surface and Coatings Technology, which has been published in final form at 10.1016/j.surfcoat.2014.02.003.

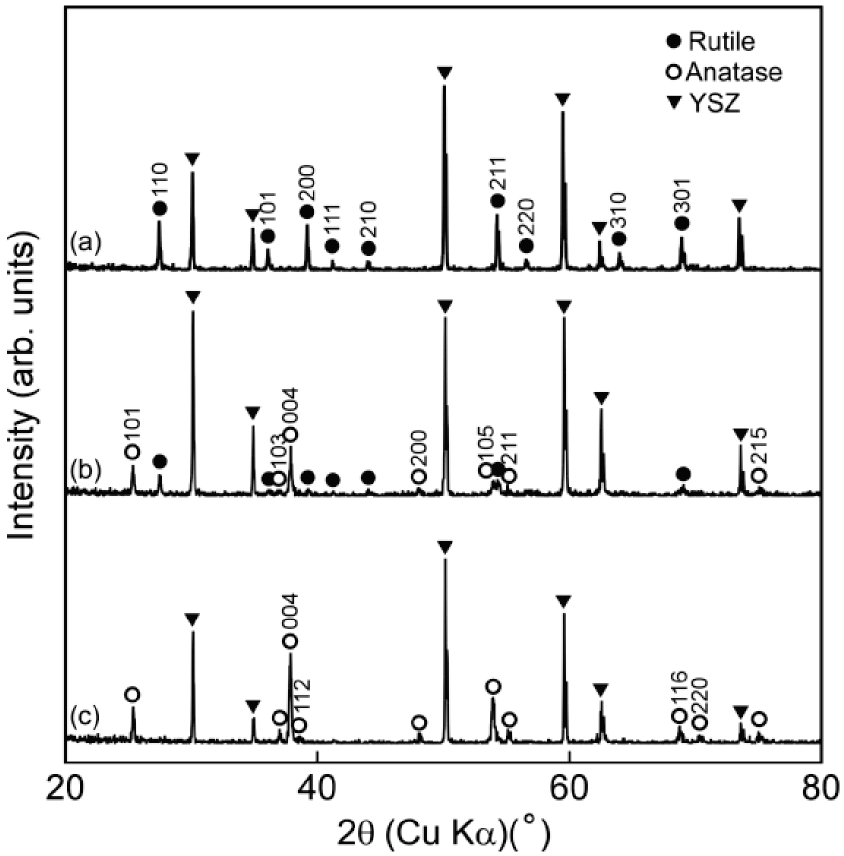

Figure 8 XRD patterns of TiO_2 films prepared using Nd:YAG laser at P_{tot} = 0.6 kPa and various T_{dep}: 1047 K (a), 1072 K (b) and 1142 K (c).

This is the accepted version of the article submitted to Surface and Coatings Technology, which has been published in final form at 10.1016/j.surfcoat.2014.02.003.

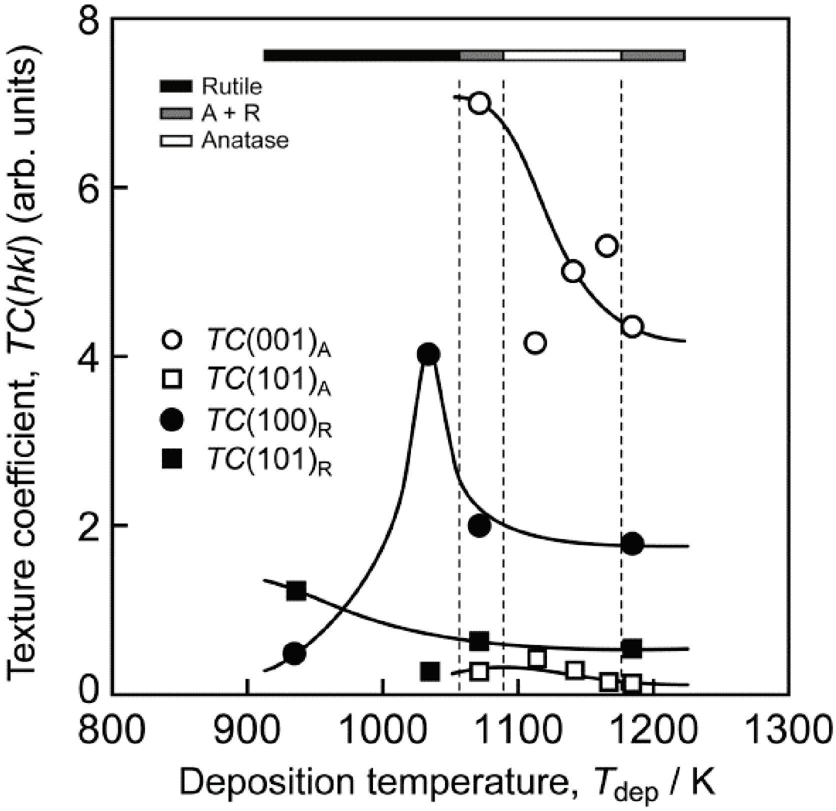

Figure 9 Effect of T_{dep} on $TC(hkl)$ of TiO_2 films prepared using Nd:YAG laser at P_{tot} = 0.6 kPa.

This is the accepted version of the article submitted to Surface and Coatings Technology, which has been published in final form at 10.1016/j.surfcoat.2014.02.003.

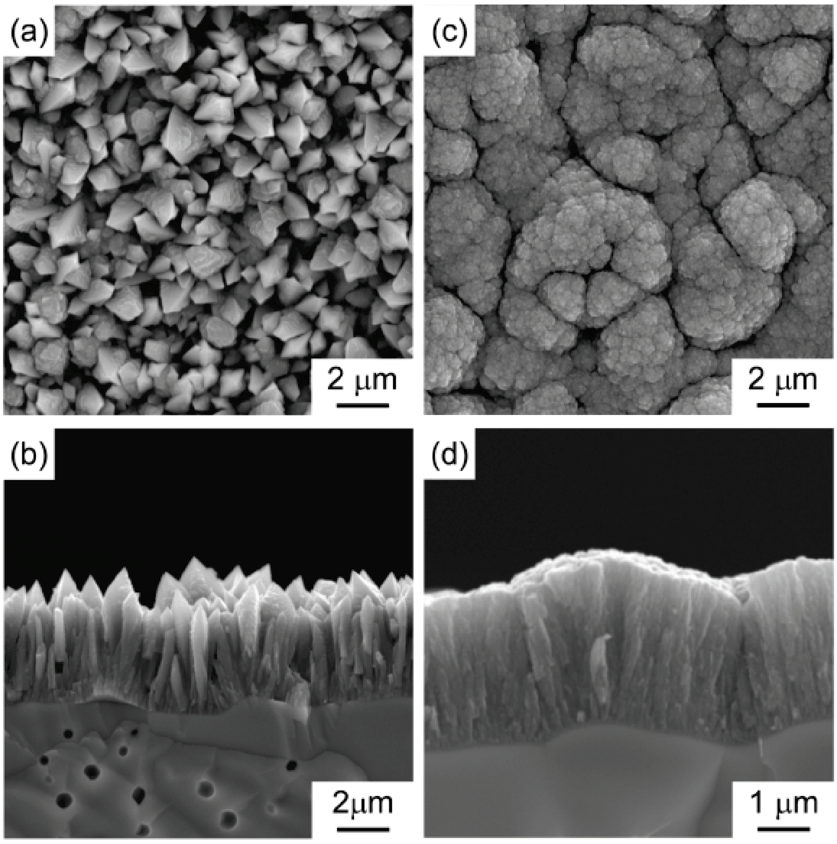

Figure 10 Surface and cross-sectional SEM images of TiO_2 films prepared by Nd:YAG laser at $P_{to\ t}$= 0.6 kPa and different T_{dep}: 1035 K (a, b) and 1142 K (c, d).

This is the accepted version of the article submitted to Surface and Coatings Technology, which has been published in final form at 10.1016/j.surfcoat.2014.02.003.

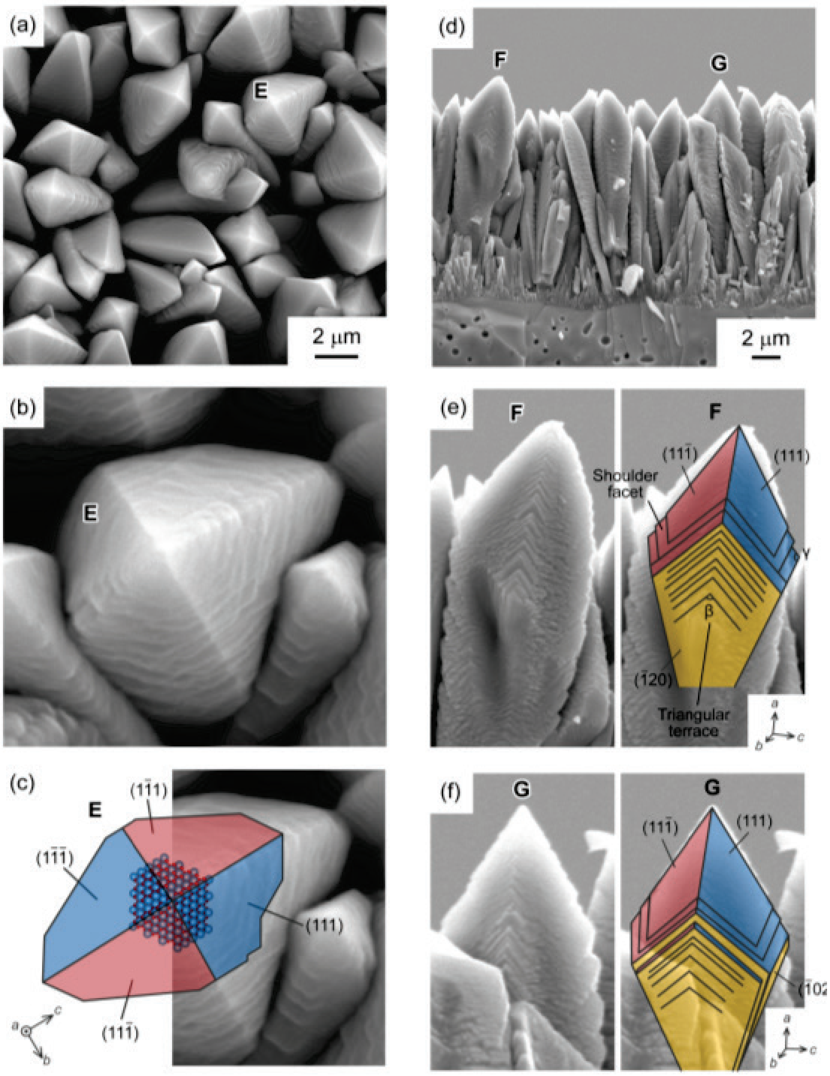

Figure 11 The feather-like structure of (100)-oriented rutile TiO_2 film prepared at P_{tot} = 0.4 kPa and T_{dep} = 1047 K: surface (a-c) and cross-section (d-f). A schematic of crystal shapes drawn by VESTA are overlaid on SEM images (c), (e) and (f).

This is the accepted version of the article submitted to Surface and Coatings Technology, which has been published in final form at 10.1016/j.surfcoat.2014.02.003.

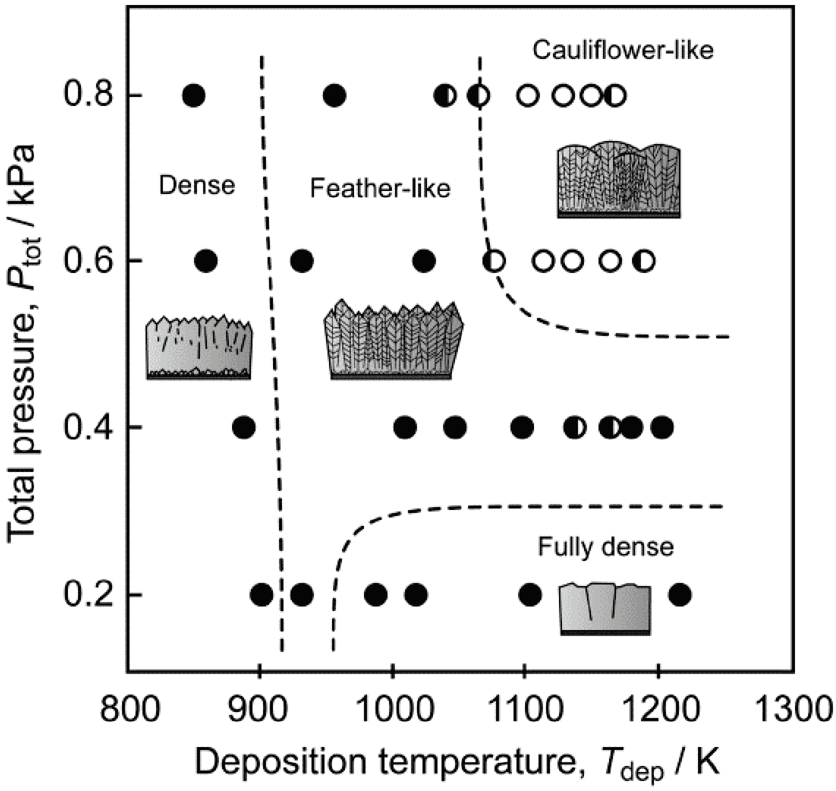

Figure 12 Effect of T_{dep} and P_{tot} on the phase and microstructure of TiO_2 films prepared by Nd:YAG laser. Filled, half-filled and open circles indicate rutile, mixture and anatase formation, respectively.

This is the accepted version of the article submitted to Surface and Coatings Technology, which has been published in final form at 10.1016/j.surfcoat.2014.02.003.

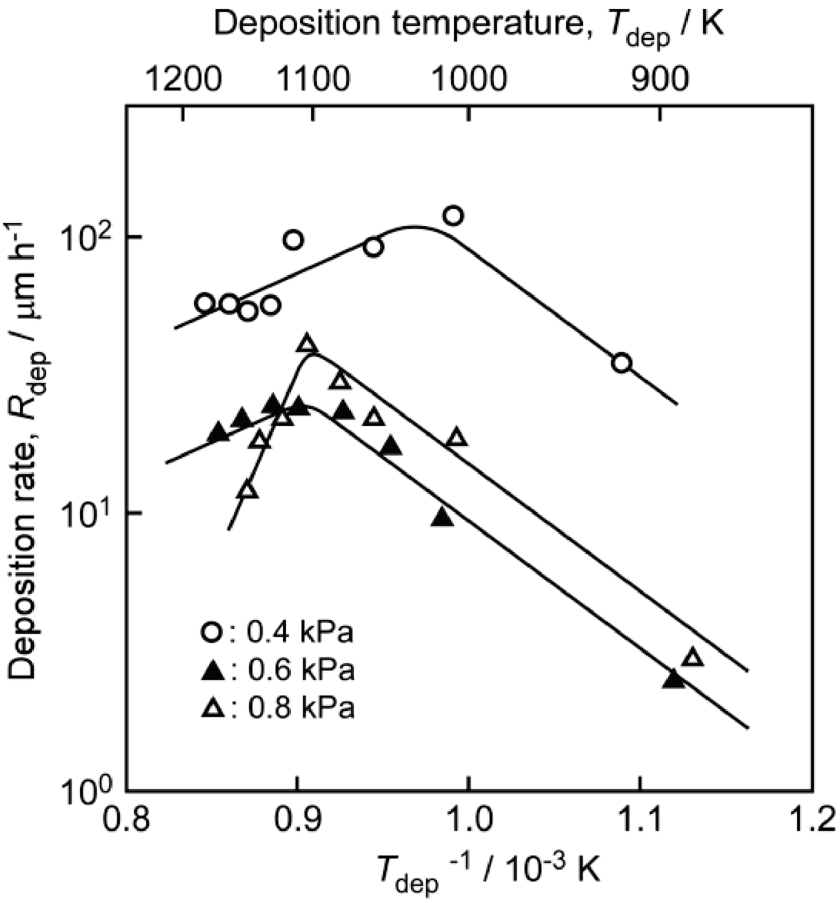

Figure 13 Effect of T_{dep} and P_{tot} on R_{dep} of TiO_2 films prepared using Nd:YAG laser.

This is the accepted version of the article submitted to Surface and Coatings Technology, which has been published in final form at 10.1016/j.surfcoat.2014.02.003.

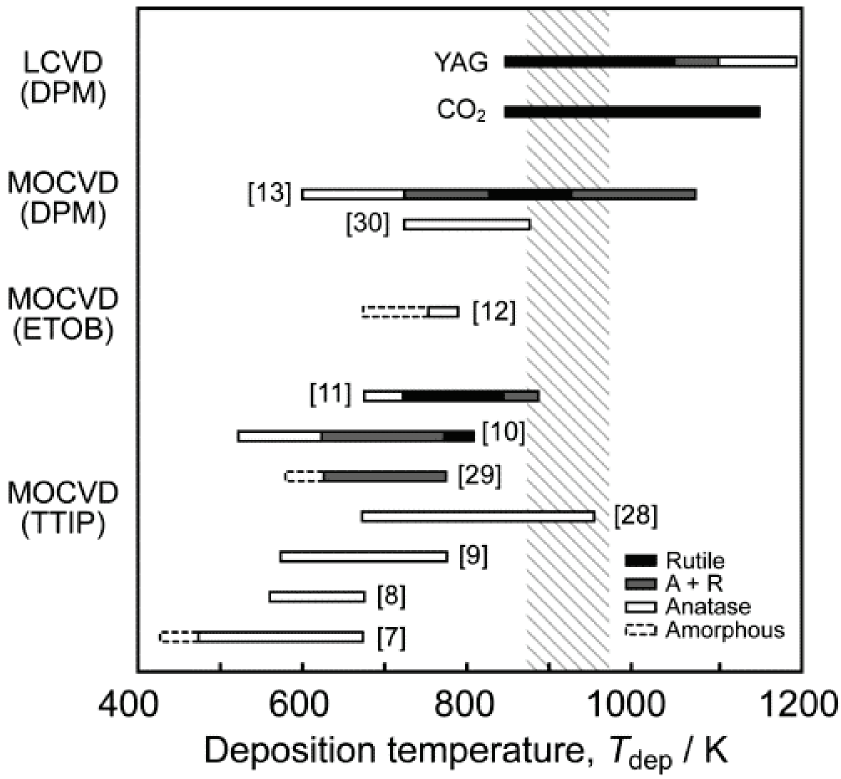

Figure 14 Anatase and rutile formation in TiO_2 films prepared by MOCVD and present LCVD. TTIP: titanium tetraisopropoxide, ETOB: titanium ethylacetoacetate, DPM: titanium dipivaloylmethanate. Hatched region indicate the temperatures for anatase-to-rutile transition [4].